J. Micromech. Microeng. **17** (2007) 2224–2230 doi:10.1088/0960-1317/17/11/008

Microwave dielectric heating of fluids in an integrated microfluidic device

Jayna J Shah[1,2], Siddarth G Sundaresan[1], Jon Geist[3], Darwin R Reyes[2], James C Booth[4], Mulpuri V Rao[1] and Michael Gaitan[2]

[1] George Mason University, Department of Electrical and Computer Engineering, 4400 University Drive, Fairfax, VA 22030, USA
[2] National Institute of Standards and Technology, Semiconductor Electronics Division, 100 Bureau Drive Stop 8120, Gaithersburg, MD 20899, USA
[3] Sequoyah Technology, LLC., 4410 Winding Oak Drive, Olney, MD 20832, USA
[4] National Institute of Standards and Technology, Electromagnetics Division, 325 Broadway, Boulder, CO 80305, USA

E-mail: gaitan@nist.gov

Received 30 March 2007, in final form 2 April 2007
Published 3 October 2007
Online at stacks.iop.org/JMM/17/2224

Abstract
The ability to selectively and precisely control the temperature of fluid volumes ranging from a few microliters to sub-nanoliters in microfluidic networks is vital for a wide range of applications in micro total analysis systems (μTAS). In this work, we characterize and model the performance of a thin film microwave transmission line integrated with a microfluidic channel to heat fluids with relevant buffer salt concentrations over a wide range of frequencies. A microchannel fabricated in poly(dimethylsiloxane) (PDMS) is aligned with a thin film microwave transmission line in a coplanar waveguide (CPW) configuration. The electromagnetic fields localized in the gap between the signal and ground lines of the transmission line dielectrically heat the fluid in the selected region of the microchannel. Microwave *S*-parameter measurements and optical fluorescence-based temperature measurements are used with a theoretical model developed based on classical microwave absorption theory to fully characterize the temperature rise of the fluid. We observe a 0.95 °C mW^{-1} temperature rise at 15 GHz and confirm that the temperature rise of the fluid is predominantly due to microwave dielectric heating.

(Some figures in this article are in colour only in the electronic version)

1. Introduction

Rapid, selective and uniform heating of fluid volumes ranging from a few microliters to as low as a few nanoliters is vital for a wide range of microfluidic applications. For example, DNA amplification by polymerase chain reaction (PCR) is critically dependent on rapid and precise thermocycling of reagents at three different temperatures between 50 °C and 95 °C [1]. Another important and related application, temperature-induced cell lysis, necessitates fluid temperature in the vicinity of 94 °C [2]. Other potential applications of heating in a microchip format include organic/inorganic chemical synthesis, the investigation of reaction kinetics, and biological studies to name a few.

A number of conduction-based heating approaches have been reported for microfluidic systems that include embedded resistive heaters, peltier elements or joule heating under electroosmotic flow conditions [3–6]. Generally speaking, these methods require physical contact between a fluid and a heated surface to transfer heat from that surface to the fluid. In microfluidic devices, when the fluid volumes approach nanoliters, heating rates will be potentially limited by the added thermal mass of the substrates used for heat transfer, and not by the fluid volume. The transfer of heat in such a manner

can also result in the heating of large substrate areas creating spatial limitations for the integration of multiple analysis functions on a single substrate. Alternatively, Giordano *et al* have demonstrated the use of a tungsten lamp as an IR source for rapidly heating small volumes of solution in a microchip format [7]. Although fast cycling times have been attained, the task of multiplexing with this approach still remains a challenge.

Conversely, microwave dielectric heating is a fundamentally different approach because of its preferential heating capability and non-contact delivery of energy. It is based on direct volumetric delivery of heat, i.e., microwave energy can be delivered to the sample with no interference from the substrate material [8]. Enhanced thermocycling rates and reduced reaction times compared to conventional techniques can be achieved because of the inertialess nature of microwave heating [9]. Heating can also be made spatially selective by confining the electromagnetic fields to specific regions in the microfluidic network. Further, the dielectric properties of the fluid can also be exploited to deliver heat using signal frequency as a control parameter in addition to the power. The microwave power absorbed per unit volume in a dielectric material is given by $P_v = \sigma E^2$, where $\sigma = 2\pi f \varepsilon_o \varepsilon''$ is the dielectric conductivity of the material, f is the frequency in hertz, ε_o is a constant called the permittivity of free space, ε'' is the imaginary part of the complex permittivity of the material that depends on the frequency and temperature and E is the electric field strength in volts per meter within the material [8]. Interestingly, the conductivity of some electrolytes is relatively independent of ion concentration over a small region of microwave frequencies [10]. Therefore, such solutions can be heated with microwaves independently of their ionic strength. This characteristic of microwave dielectric heating is particularly advantageous when the salt concentration of the solution is not known *a priori*, as would be a common case.

The use of microwave heating has been demonstrated for a variety of applications including drug discovery [11], PCR [12, 13], isolation of DNA [14] and heating of biological cells [15]. However, macroscale microwave applicators have been utilized, which are potentially unsuitable for portable microfluidic devices. Recently, there has been much interest in integrating miniaturized microwave heating elements, in the form of transmission lines, with microfluidic channels for on-chip heating applications [16]. Sklavonous *et al* have presented thermocycling of water and PCR buffer solution in a microfluidic well designed to terminate microwave energy [17]. Even though the reported results provide strong foundation for further development of this technology, much work is required to make this technology commercially viable.

In this work, we characterize and model the performance of a thin film microwave transmission line integrated with an elastomeric microfluidic channel to heat fluids with differing salt concentrations over a wide range of frequencies. A coplanar waveguide (CPW) is a commonly used planar microwave transmission line. It has been integrated with a fluidic microchannel for on-chip dielectric permittivity and spectroscopy measurements [18, 19]. In this paper, we demonstrate the use of thin-film CPW for on-chip microwave heating of fluids in the microchannel. We perform two-port scattering (S) parameter measurements of the device when the microchannel is empty and filled with various fluids and use the results to characterize the absorption of the microwave power by the device as a function of frequency. The S-parameter data are also used to develop a first-order analytic model of the microwave power absorption in low reflectance, lossy transmission lines such as the one utilized in this work. From the model, we extract several parameters such as the microwave power absorbed by the fluid and by the CPW conductors and use them to evaluate the efficiency of this heating method for microfluidic applications. Finally, we measure the fluid temperature at various microwave frequencies using a fluorescence detection technique, and also perform a fit of the predicted temperature obtained using our model to the measured temperature and show that good agreement is found.

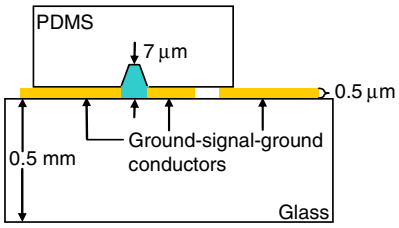

Figure 1. Schematic of a cross-section of a coplanar waveguide (CPW) transmission line integrated with a poly(dimethylsiloxane) (PDMS) microchannel for microwave dielectric heating of fluids. The CPW conductors are 1.5 cm long; the single conductor is 140 μm wide and it is separated by a 25 μm gap on either side from 300 μm wide ground conductors. The microchannel consists of a trapezoidal cross section defined by a silicon template and it is 7 μm deep, 25 μm wide at the bottom and 3.62 mm long.

2. Experimental details[5]

2.1. Materials

Silicon wafers were obtained from Nova Electronic Materials, Ltd (Carrollton, TX). PDMS (Sylgard 184) and Pyrex® 7740 borosilicate glass wafers were obtained from Dow Corning (Midland, MI). PDMS was mixed and cured according to the manufacturer's specifications. Rhodamine B (laser grade) was purchased from Acros Organics USA (Morris Plains, NJ).

2.2. Device fabrication

A schematic of a cross-sectional view of the device fabricated in this study is shown in figure 1. It consisted of a CPW integrated with an elastomeric microfluidic channel. The CPW was comprised of a 140 μm wide signal conductor separated by a 25 μm gap on either side from 300 μm wide ground conductors. The CPW conductors, 1.5 cm long, were formed by thermally evaporating Cr/Au (10 nm/500 nm) on a 0.5 mm thick glass wafer and using a standard lift-off metallization process. The microchannel was patterned into

[5] Certain commercial equipment, instruments or materials are identified in this paper to specify adequately the experimental procedure. Such identification does not imply recommendation or endorsement by the National Institute of Standards and Technology, nor does it imply that the materials or equipment identified are necessarily the best available for the purpose.

poly(dimethylsiloxane) (PDMS) by soft lithography [20]. It consisted of a trapezoidal cross section defined by a silicon template and was 7 μm deep, 25 μm wide at the bottom and 3.62 mm long. The microchannel was attached by contact adhesion on top of the CPW and approximately centered along the length of the CPW conductors. The microchannel was carefully aligned in the lateral direction over the CPW such that its bottom surface coincided with the separation between the signal conductor and one of the ground conductors (the region of high electric field strength).

2.3. Device characterization

Two types of measurements were taken to characterize the device: scattering (*S*) parameter and temperature. Precision air coplanar probes obtained from Cascade Microtech, Inc. (Moorestown, NJ) were used to convert from the coaxial geometry of the test set to the coplanar geometry used for the CPW transmission line. *S*-parameters relate the forward and reflected traveling waves in a transmission medium and can be used to understand the power flow as a function of frequency. We have used *S*-parameters in conjunction with the conservation of energy to model absorption of microwave power and to predict the fluid temperature based on the absorbed power. The predicted temperature was then fitted to the measured temperature to determine heating efficiency.

2.3.1. S-parameter measurements. *S*-parameters, the transmission and reflection coefficients, of the device shown in figure 1 were obtained using an HP 8510C vector network analyzer connected to an HP 8517B S-parameter test set. An HP 83650B signal generator was used to source the microwave continuous wave (CW) signal. The measurements were calibrated using commonly used thru-reflect-line (TRL) calibration utilized for on-wafer characterization of CPW-based devices [21]. The experiments in this work were performed with deionized (DI) H_2O and with fluids of two different salt concentrations: 0.9% NaCl solution and 3.5% NaCl solution.

2.3.2. Temperature measurements. The fluid temperature was obtained by measuring the temperature dependent fluorescence intensity of a dilute fluorophore added to the fluid and comparing it to the calibrated fluorescence intensity at a known temperature according to the procedures previously published [22]. Specifically, an aqueous solution of 0.2 mmol L^{-1} Rhodamine B prepared in a 19 mmol L^{-1} carbonate buffer was used for making temperature measurements. The chemical properties of Rhodamine B have been studied extensively [23, 24], and its temperature-sensitivity has been utilized in a variety of applications [25, 26]. Fluorescence imaging of the Rhodamine B solution in this work was performed using an inverted laser-induced fluorescence microscope equipped with a long working distance 20× objective, a mercury arc lamp, an appropriate filter set (excitation, 500–550 nm; emission, >565 nm) and a video camera. All temperature measurements were conducted on the stage of a microscope. A constant microwave power was applied at the input port of the CPW using a signal generator. Microwave power was terminated by connecting an HP 8485B power sensor at the output port of the CPW device while a HP 437B power meter connected to the power sensor was used to measure microwave power. The fluorescence intensity was calibrated using the following technique. A thin-film resistor (8 nm Cr/260 nm Au) of an equivalent footprint (25 μm wide and 3.6 mm long) as the microfluidic channel was patterned on a glass substrate using photolithographic techniques. The microfluidic channel was then aligned on the top of the resistor and filled with an aqueous solution of Rhodamine B dye. The resistor was then heated using a dc power source (Keithley 2001) while the fluorescence intensity of the dye and the resistance of the resistor were recorded. The temperature coefficient of resistance, which had been determined empirically, was used to determine the temperature–intensity relationship.

3. Results and discussion

We performed two experiments to evaluate the performance of the CPW devices for heating in the microchannel environment: the first characterizes the frequency response of the device, which is also used to obtain absorption ratios of the devices with empty and fluid-filled microchannels, and the second measures fluid temperature at various microwave frequencies. We have used the results obtained from the first experiment to derive a power absorption model to find the distribution of the incident microwave power in different absorbing structures of the device.

3.1. S-parameter measurements

The amplitude of the reflection coefficients (S_{11}) and transmission coefficients (S_{21}) from 0.3 GHz to 40 GHz for the device with an empty channel as well as for the fluid-filled channels are shown in figures 2(*a*) and (*b*), respectively. In comparison with the empty channel device, S_{11} is reduced for the device with fluid-filled channel and it approaches that of an empty channel for frequencies above 10.5 GHz. The decrease in S_{11} of the fluid-filled devices below 10.5 GHz which indicate good impedance matching conditions are apparently fortuitous. S_{11} is also found to be almost independent of the ionic concentration of the fluid. The localized peak and trough features observed in S_{11} are likely interference effects due to reflections at the probe–CPW interfaces and the CPW/air–CPW/fluid interfaces [19]. S_{21}, as seen from figure 2(*b*), decreases with increasing frequency for the devices with both the empty and fluid-filled channels. We believe that the apparent low transmission coefficient of the empty-channel device is likely due to the smaller than optimum thickness of the CPW conductors (0.5 μm). The difference in S_{21} between the empty and fluid-filled channels becomes more pronounced at higher frequencies (>5 GHz). S_{21} of the fluid-filled devices is smaller compared to the empty-channel device due to the additional attenuation caused by the absorption of the microwave energy in the water.

Figure 3 shows percent absorption ratios (the fraction of the incident power absorbed by the device) as a function of frequency for the devices with empty and fluid-filled microchannels. The absorption ratio, *A*, is calculated from the S-parameter data shown in figure 2 and using equation (1):

$$A = 1 - R - T \tag{1}$$

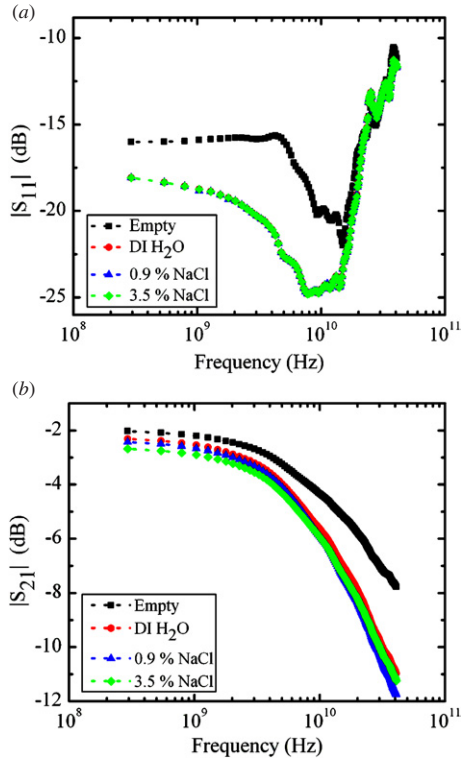

Figure 2. (*a*) Measured reflection coefficients $|S_{11}|$ of the device. (*b*) Measured transmission coefficients ($|S_{21}|$) of the device. (■) Empty microchannel, (●) microchannel filled with deionized H_2O, (▲) microchannel filled with 0.9% NaCl, (♦) microchannel filled with 3.5% NaCl.

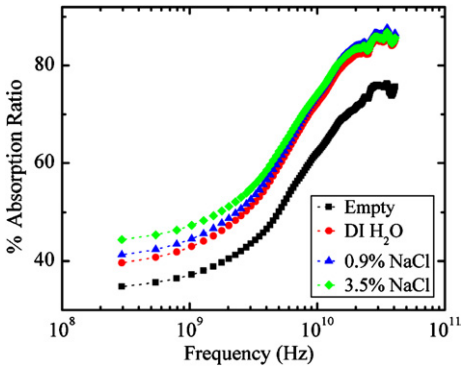

Figure 3. The percent absorption ratios (the fraction of the incident microwave power absorbed by the device) as a function of frequency. The absorption ratio, A, was calculated from the measured transmission and reflection coefficients using $A = 1 - R - T$. (■) Empty microchannel, (●) microchannel filled with deionized H_2O, (▲) microchannel filled with 0.9% NaCl, (♦) microchannel filled with 3.5% NaCl.

where R (the reflection coefficient) $= |S_{11}|$, T (the transmission coefficient) $= |S_{21}|$ and $S_{ij}(\mathrm{dB}) = 10\log_{10}|S_{ij}|$. It should be noted that the absorption ratio is dependent on the position of the microchannel over the length of the waveguide. In other words, S_{21} would not be equal to S_{12} and the device would function as a non-reciprocal two-port network unless the microchannel is precisely centered over the length of the waveguide. The absorption ratio obtained for the device with empty channel (■) is due to ohmic dissipation in the thin-film CPW, which can be modeled by an attenuation constant, α_{cpw}, which corresponds to 2.86 dB cm^{-1} at 10 GHz. The attenuation constant of PDMS is assumed to be negligible because of the relatively low values of loss tangent (the ability of a material to convert stored electrical energy into heat) at microwave frequencies [27]. An increase in A observed with increasing frequency for the empty channel device (■) is expected from the dependence of skin depth on frequency. The absorption ratio for the fluid filled devices (●, ▲, and ♦) is greater for all frequencies measured in comparison with the empty channel device (■), due to microwave absorption in water and also ionic absorption in the ionic solutions. The data also exhibit a dependence of A on ionic concentration at lower frequencies as would be expected due to ionic conductivity, while the data at higher frequencies show that A is approximately independent of ionic concentration, as would be expected due to dielectric conductivity. This trend is in agreement with theory [10].

3.2. Power absorption model

It seems from figure 3 that the simplest approximation to the fraction of the incident microwave power absorbed in the fluid is the difference between the power absorbed by the full-channel and empty-channel devices (for the case of water-filled device, $A_{\mathrm{H_2O}} - A_{\mathrm{empty}}$ in figure 3). However, the various microwave power absorption models described in [28] show that this simple approximation greatly underestimates the actual fraction absorbed in the fluid. In this work, we have chosen a simple model, alpha absorption model, to extract the fraction of the incident power absorbed in the fluid. This model is also used to differentiate microwave heating of the fluid from conductive heating due to ohmic heating of the CPW conductors. As shown in figure 4(*a*), it is constructed by assuming that the PDMS completely covers the CPW and by partitioning the CPW into three regions: a center region that interacts with the fluid in the microchannel and two ends that have no microchannel over them. The lengths of each of the three regions are defined by the center region, z_2, 0.36 cm long and two end regions, z_1 and z_3, 0.57 cm long. The reflectance at the interface between the regions is assumed to be negligible, and the transmission coefficient, T, is modeled by equation (2):

$$T = (1 - R) \times \mathrm{e}^{-2\alpha_{\mathrm{cpw}} z_1} \times \mathrm{e}^{-2\alpha_{\mathrm{cpw}} z_2} \times \mathrm{e}^{-2\alpha_w z_2} \times \mathrm{e}^{-2\alpha_{\mathrm{cpw}} z_3}. \quad (2)$$

The derivation of this equation is based on exponential attenuation of microwave power in the direction of propagation where the rate of decay with distance is described by the attenuation constant, α. Because of the presence of water in the center region, it should be noted that the attenuation due to water, α_w, is added to the attenuation due to CPW, α_{cpw}. Equation (2) is then used to derive α_{cpw} and α_w as follows. First, α_{cpw} is derived for the empty channel device by setting α_w equal to zero into equation (2) and substituting the measured values of T and R for the empty channel device. Next, this value of α_{cpw} is substituted into equation (2) along with the measured values of T_f and R_f, which are T and R for the water filled device. The resulting equation is solved for α_w, which is found to be 3.68 dB cm^{-1} at 10 GHz. The absorption

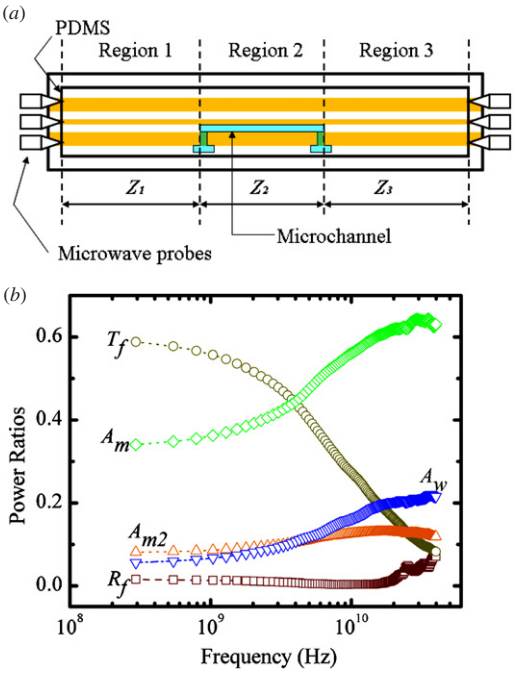

Figure 4. (*a*) Top view of a coplanar waveguide (CPW) integrated with a poly(dimethylsiloxane) (PDMS) microchannel consisting of three regions, a center region with the microchannel and two end regions without the microchannel. (*b*) The distribution of the incident microwave power in different absorbing structures of deionized H_2O filled device as obtained from the alpha absorption model. T_f, R_f are the transmission and reflection coefficients of the water-filled device, respectively; A_m, A_{m2}, A_w are the absorption ratio of the CPW conductors, the absorption ratio of the CPW conductors in the region with the microchannel and the absorption ratio of the water, respectively.

ratio for the central region of the water filled channel, A_2, is calculated as

$$A_2 = (1 - R_f) \times (e^{-2\alpha_{cpw} z_1}) \times (1 - e^{-2(\alpha_{cpw}+\alpha_w) z_2}). \quad (3)$$

Finally, the absorption ratios of the water, A_w, and CPW conductors, A_{m2}, in the center region are calculated by $A_w = [\alpha_w/(\alpha_{cpw} + \alpha_w)]A_2$ and $A_{m2} = A_2 - A_w$, respectively.

Equations (2) and (3) are first-order approximations. For impedance matched conditions, the equations show that A_w is dependent on the position of the microchannel along the length of the CPW with a maximum occurring at the source end because the transmitted power attenuates exponentially along the transmission line. Further, A_w decreases exponentially along the length of the microchannel. Therefore, there is a design tradeoff between the microchannel length, its position relative to the source and the frequency of operation to obtain a uniform temperature rise and efficient absorption of microwave power. Figure 4(*b*) shows the distribution of the incident microwave power in different absorbing structures of the deionized H_2O filled device. It shows that A_w increases with frequency in agreement with theory because the power absorbed by water per unit volume is proportional to $f\varepsilon''$, as calculated from Franks [29]. It also shows that the absorption by the metal in the central region (A_{m2}) competes with the absorption by the water (A_w). At low frequencies (< 3.5 GHz), A_{m2} is slightly higher than A_w. The difference between the two

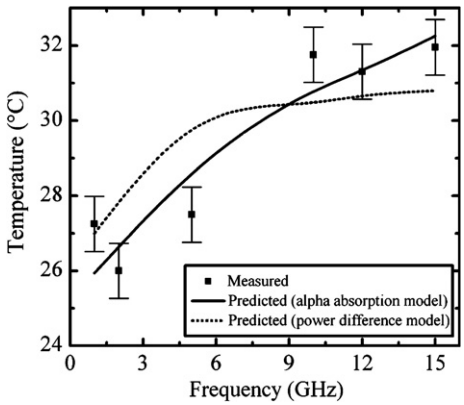

Figure 5. The measured temperature (■) of an aqueous solution of 0.2 mmol L^{-1} Rhodamine B in a 19 mmol L^{-1} carbonate buffer as a function of frequency. The solid line indicates the predicted temperature calculated from the alpha absorption model, and the dashed line was calculated by employing the power difference model.

becomes negligible as the frequency increases further, and A_w starts to dominate as the frequency exceeds approximately 8 GHz. This can be explained by the differences in the attenuation constants. For instance, α_w is 1.3 times as high as α_{cpw} at 10 GHz. It can be observed from figure 4(*b*) that the fraction of the incident power absorbed by the CPW conductors, A_m, is noticeably high over the entire frequency range measured. This results in the ohmic heating of the CPW conductors, which is also expected to contribute to the temperature rise of the fluid. However, based on the incident power absorbed by the CPW conductors in the center region, A_{m2}, a worst-case first order analytic calculation [30] of the contribution of the metal heating to water heating shows that the power dissipated in the CPW contributes less than 20% of the total heating observed in the microchannel.

3.3. Temperature measurements

The points (■) in figure 5 show the fluid (aqueous solution of Rhodamine B) temperature measured at various microwave frequencies. The applied power was kept constant at 10 mW. The temperature was measured ∼250 ms after turning on the microwave power, which was approximated to be within 5% of quasi-thermal equilibrium. The error bars indicate the pooled standard deviation over all measurements for two instances at each frequency added with the estimated standard deviation (0.5 °C) of the room temperature (22.5 °C). The observed temperature rise was 0.88 °C mW^{-1} at 12 GHz and 0.95 °C mW^{-1} at 15 GHz.

The temperature can also be calculated from the energy absorbed in the water during the heating period dt using equation (4):

$$dT = \frac{P_v\, dt}{\rho C_p} = \frac{K_e I A_w\, dt}{\rho C_p V} \quad (4)$$

where ρ and C_p are the density and heat capacity of water, respectively, at appropriate temperature, I is the incident microwave power, A_w is the fraction of the incident power absorbed in the water as shown in figure 4(*b*), and V is the volume of water in the microchannel. K_e is the channel-heating efficiency, which is defined as the fraction of energy

absorbed in the water during the time dt that remains in the water. The rest of the energy absorbed in the water during the time dt is conducted into the substrate. The value of K_e cannot be easily obtained from the geometry and thermal properties of the channel and substrate due to the unknown contact thermal resistance (Kapitza resistance) between the water and the hydrophobic surface of the substrate [31]. Rather than attempt to calculate the value of K_e, it was adjusted in a least-squares fit of the predictions of equation (4) to the measured data points (■) in figure 5. The solid line in figure 5 indicates the predicted temperature calculated using A_w obtained from figure 4 (alpha absorption model), and the dashed line indicates the predicted temperature calculated using A_w obtained from the power difference model ($A_{H_2O} - A_{empty}$). It is clear from the results of fitting the predictions of the two different absorption models that the alpha absorption model provides a better fit to the measured data. Further, the heating efficiency obtained from the alpha absorption model indicates that only 5% of the total heat (time integral of the absorbed power) was stored in the fluid while the rest was lost to the surroundings (PDMS and glass). Because the ratio of stored heat to lost heat increases with decreasing heating time, it is possible to confine most of the heat to the fluid and heat it to a higher temperature by increasing the microwave power and decreasing the heating period simultaneously.

4. Conclusions

The ability to rapidly and selectively control temperature within a microchannel environment is crucial for many fluidic applications including high-efficiency PCR and temperature-induced cell lysis. In this paper, we have demonstrated localized microwave dielectric heating of fluids at micrometer scale geometry using an integrated planar microwave transmission line as a power source. The measured temperature is shown to increase with increasing frequency in agreement with theory. The device used in this study offers several advantages. It is simple, easy to use and fabricate. The planar structure of the transmission line used as a power source lends itself to easy integration with the microchannel and allows for optical interrogation of the microchannel with widely used fluorescence microscopy techniques. The performance of the CPW for heating could be substantially improved by applying high power pulses over shorter heating times, using a lower thermal diffusivity substrate than glass and increasing the gap width and thickness of the CPW conductors.

We have developed a microwave power absorption model to understand power distribution through the device and to differentiate microwave heating of the fluid from conductive heating of the fluid because of microwave power absorption in thin-film CPW conductors. We have used this power absorption model to analyze the experimental data and demonstrated that the temperature rise of fluid is predominantly due to the absorbed microwave power. We believe this model can be useful for evaluating the performance of various complex and lossy transmission line configurations, such as CPW, microstrip lines, or striplines, for heating fluid in the microchannel environment.

Finally, we believe that the microwave dielectric heating approach will be of particular use in rapid thermocycling applications and will lead to new applications exploiting heating in a microfluidic environment. Current studies in our laboratory are addressing the use of such heaters for single-use, disposable and integrated microfluidic systems.

Acknowledgments

This work is supported by the Office of Science and Technology of the National Institute of Justice. Device fabrication for this work was performed at the NIST Semiconductor Electronics Division Microfabrication Process Facility managed by Russell Hajdaj. SGS was supported by GMU's School of Information Technology and Engineering graduate research assistant scholarship. Financial support for JJS was provided by NIST under grant no 60NANB4D1132. The authors thank D Blackburn, B Polk and D Ross for helpful discussions during the course of this work.

References

[1] Kopp M U, de Mello A J and Manz A 1998 Chemical amplification: continuous-flow PCR on a chip *Science* **280** 1046–8
[2] Waters L C, Jacobson S C, Kroutchinina N, Khandurina J, Foote R S and Ramsey J M 1998 Microchip device for cell lysis, multiplex PCR amplification, and electrophoretic sizing *Anal. Chem.* **70** 158–62
[3] Lee C Y, Lee G B, Lin J L, Huang F C and Liao C S 2005 Integrated microfluidic systems for cell lysis, mixing/pumping and DNA amplification *J. Micromech. Microeng.* **15** 1215–23
[4] Maltezos G, Johnston M and Scherer A 2005 Thermal management in microfluidics using micro-Peltier junctions *Appl. Phys. Lett.* **87** 1541051–3
[5] de Mello A J, Habgood M, Lancaster N L, Welton T and Wootton R C R 2004 Precise temperature control in microfluidic devices using Joule heating of ionic liquids *Lab Chip* **4** 417–9
[6] Liu P, Seo T S, Beyor N, Shin K J, Scherer J R and Mathies R A 2007 Integrated portable polymerase chain reaction-capillary electrophoresis microsystem for rapid forensic short tandem repeat typing *Anal. Chem.* **79** 1881–9
[7] Giordano B C, Ferrance J, Swedberg S, Huhmer A F R and Landers J P 2001 Polymerase chain reaction in polymeric microchips: DNA amplification in less than 240 seconds *Anal. Biochem.* **291** 124–32
[8] Bengtsson N E and Ohlsson T 1974 Microwave heating in the food industry *Proc. IEEE* **62** 44–55
[9] Bykov Y V, Rybakov K I and Semenov V E 2001 High-temperature microwave processing of materials *J. Phys. D: Appl. Phys.* **34** R55–75
[10] Wei Y Z and Sridhar S 1990 Dielectric-Spectroscopy up to 20 Ghz of LiCl/H_2O Solutions *J. Chem. Phys.* **92** 923–8
[11] Kappe C O and Dallinger D 2006 The impact of microwave synthesis on drug discovery *Nat. Rev. Drug Discov.* **5** 51–63
[12] Fermer C, Nilsson P and Larhed M 2003 Microwave-assisted high-speed PCR *Eur. J. Pharm. Sci.* **18** 129–32
[13] Auroux P A, Shah J J, Booth J, Rao M V, Locascio L E and Gaitan M 2006 Microfluidic method for thermal cycling by microwave dielectric heating *Proc. Micro Total Anal. Syst.* **2** 1465–7
[14] Goodwin D C and Lee S B 1993 Microwave miniprep of total genomic DNA from fungi, plants, protists and animals for PCR *Biotechniques* **15** 438
[15] Nikawa Y, Yamamoto K, Izumidate S and Kubota N 1996 An Irradiation System of Pulsed Modulation Microwaves to Culture Cells *18th Int. Conf. IEEE Eng. Med. Biol. Soc.* vol 5 pp 1865–6

[16] Sundaresan S G, Polk B J, Reyes D R, Rao M V and Gaitan M 2005 Temperature control of microfluidic systems by microwave heating *Proc. Micro Total Anal. Syst.* **1** 657–9
[17] Sklavounos A, Marchiarullo D J, Barker S L R, Landers J P and Barker N S 2006 Efficient miniaturized systems for microwave heating on microdevices *Proc. Micro Total Anal. Syst.* **2** 1238–40
[18] Booth J C, Mateu J, Janezic M, Baker-Jarvis J and Beall J A 2006 Broadband permittivity measurements of liquid and biological samples using microfluidic channels *IEEE MTT-S Int. Microw. Symp.* 1750–3
[19] Facer G R, Notterman D A and Sohn L L 2001 Dielectric spectroscopy for bioanalysis: from 40 Hz to 26.5 GHz in a microfabricated wave guide *Appl. Phys. Lett.* **78** 996–8
[20] Duffy D C, Schueller O J A, Brittain S T and Whitesides G M 1999 Rapid prototyping of microfluidic switches in poly(dimethyl siloxane) and their actuation by electro-osmotic flow *J. Micromech. Microeng.* **9** 211–7
[21] Engen G F 1997 A (historical) review of the six-port measurement technique *IEEE Trans. Microw. Theor. Tech.* **45** 2414–7
[22] Ross D, Gaitan M and Locascio L E 2001 Temperature measurement in microfluidic systems using a temperature-dependent fluorescent dye *Anal. Chem.* **73** 4117–23
[23] Arbeloa T L, Estevez M J T, Arbeloa F L, Aguirresacona I U and Arbeloa I L 1991 Luminescence properties of Rhodamines in water–ethanol mixtures *J. Lumin.* **48–9** 400–4
[24] Kubin R F and Fletcher A N 1982 Fluorescence quantum yields of some rhodamine dyes *J. Lumin.* **27** 455–62
[25] Gallery J, Gouterman M, Callis J, Khalil G, McLachlan B and Bell J 1994 Luminescent thermometry for aerodynamic measurements *Rev. Sci. Instrum.* **65** 712–20
[26] Lemoine F, Antoine Y, Wolff M and Lebouche M 1999 Simultaneous temperature and 2D velocity measurements in a turbulent heated jet using combined laser-induced fluorescence and LDA *Exp. Fluids* **26** 315–23
[27] Tiercelin N, Coquet P, Sauleau R, Senez V and Fujita H 2006 Polydimethylsiloxane membranes for millimeter-wave planar ultra flexible antennas *J. Micromech. Microeng.* **16** 2389–95
[28] Geist J, Shah J J, Rao M V and Gaitan M 2007 Microwave power absorption in low-reflectance, complex, lossy transmission lines *J. Res. Natl. Inst. Stand. Technol.* **112** 177–89
[29] Franks F 1972 *Water: A Comprehensive Treatise* vol 1 ed F Franks (New York: Plenum)
[30] Carslaw H S and J J C 1959 *Conduction of Heat in Solids* 2nd edn (Oxford: Oxford University Press)
[31] Barrat J L and Chiaruttini F 2003 Kapitza resistance at the liquid-solid interface *Mol. Phys.* **101** 1605–10